Polym. Bull. (2014) 71:2247–2268
DOI 10.1007/s00289-014-1185-3

ORIGINAL PAPER

Long-term creep behavior of polypropylene/fumed silica nanocomposites estimated by time–temperature and time–strain superposition approaches

D. Pedrazzoli · A. Pegoretti

Received: 11 February 2014 / Revised: 15 May 2014 / Accepted: 19 May 2014 /
Published online: 25 May 2014

Abstract Nonlinear viscoelastic creep was studied on polypropylene/fumed silica nanocomposites. The free-volume theory of nonlinear viscoelastic creep was successfully applied to obtain generalized creep master curves using a tensile compliance vs. internal time superposition in the region of nonlinear viscoelasticity. Concurrently, a time–temperature superposition approach was also adopted for the construction of creep master curves. A good agreement between the time–strain and the time–temperature superposition approaches was assessed by comparing the master curves obtained from the two data reduction methods. Both approaches evidenced a remarkable stabilizing effect induced by the nanoparticles that was observed especially for higher creep stresses and at increased temperatures and, considering the correspondent superposition principle, at long loading times. At the same time, both storage and loss moduli measured through dynamic mechanical analyses, were enhanced in all nanocomposites. Activation energy values obtained from the analysis of dynamic multi-frequency tests were in good accordance with those referred to creep tests.

Keywords Polymer-matrix nanocomposites (PMCs) · Silica nanoparticles · Tensile creep · Free volume · Dynamic-mechanic analysis

Introduction

Both organic and inorganic fillers are generally added to polymers primarily for the reasons of stiffness improvement and cost reduction [1–5]. It is worth noting that in the case of micrometer particulates, high filler content (typically higher than

D. Pedrazzoli · A. Pegoretti (✉)
Department of Industrial Engineering and INSTM Research Unit, University of Trento,
via Sommarive 9, 38123 Trento, Italy
e-mail: Alessandro.Pegoretti@unitn.it

20 vol%) is generally required to bring positive effects of the fillers into play. On the other hand, this could negatively affect some other properties of the matrix polymers such as processability, appearance, density and aging performance [6]. Therefore, a composite with improved performance and low particle concentration is highly desired and nanocomposites would be competitive candidates.

Thermoplastic polymers find increasing application where they are expected to maintain dimensional stability while subjected to long-lasting constant loads. In this context, poor creep stability of the material might represent a limitation in the utilization of the component. On the other hand, recent research demonstrated how the reinforcement of thermoplastics with small amounts of nanofillers can also be effective in improving the creep stability [7–9]. For instance, the creep compliance of linear low-density polyethylene (LLDPE) was remarkably reduced by the incorporation of fumed silica nanoparticles and the degree of reduction was found to be proportional to the surface area of the nanoparticles [10]. In other cases, it was found that titania nanoparticles substantially reduced the creep compliance of nylon 66 [11–13], while alumina nanoparticles markedly decreased the compliance in polystyrene [14] and polyoxymethylene/polyurethane blends [15]. Similar results were reported regarding the viscoelastic properties of the polyimide/silica nanocomposites [16]. It is generally believed that nanoparticles can effectively restrict the motion of polymer chains, modifying the stress transfer at a nanoscale, thus inducing a better creep stability [10, 17–19].

Due to its good thermo-mechanical properties and relatively low cost, isotactic polypropylene (PP) is currently used in a variety of applications including textiles, food packaging, stationery but also in fields requiring a high structural stability, such as building construction and automotive industry. In this latter case, PP is frequently used as a matrix for the preparation of glass (or carbon) fiber reinforced composites [20]. The creep behavior of PP has been investigated in a series of papers [21–26]. Since the reported stress–strain linearity limit of PP is very low, the creep measurements under this limit remain inaccurate and impractical to be applied in the design of components [27]. A new approach was introduced by Kolarik et al. [27–29] in which the internal time—tensile compliance superposition of nonlinear creep data is applied to construct a generalized compliance curve, which corresponds to a pseudo iso-free-volume state. The internal time of a material differs from the experimental time by a factor depending on various parameters, such as the free volume, the applied strain and stress. The free volume is usually considered the key parameter, especially because the phenomenological theory of viscoelasticity [30–35] has shown that fractional free volume plays a key role in the control of the retardation (or relaxation) times in polymeric materials. Applying the free-volume approach to the nonlinear tensile creep of PP [29], PP/styrene-acrylonitrile copolymer (SAN) [24], PP/cycloolefin copolymer (COC) [28] and LLDPE/fumed silica [10], the formulae for the shift factors have been derived, which allow us to construct a generalized creep curve over a long time interval by applying the time–strain superposition (TSSP). Generalized creep compliance curves can be conveniently used for predicting the real time-dependent compliance for any selected stress within the region of reversible deformations [27]. Among the

accelerated procedures used to characterize the viscoelastic behavior in polymeric systems, the time–temperature superposition principle (TTSP) represents one of the most widely applied methods for the construction of master curves referred to a constant temperature [15, 36, 37]. Several authors demonstrated that TTSP is valid in the linear viscoelastic region for polymer and polymer composites [38, 39]. On the other hand, the existing literature points to the fact that TTSP is not valid within the nonlinear viscoelastic region due to the change in shape of the creep curve with stress levels [40, 41].

Only few reports available in the current literature describe both the stress and temperature dependence of the tensile creep response of a polymer system by the application of the TSSP and TTSP, respectively [42]. However, no reports are available to our knowledge on a detailed comparison of generalized creep curves constructed by applying the TSSP and TTSP in the region of nonlinear viscoelasticity on semicrystalline polymers such as PP.

The main objectives of this study are (1) to evaluate the effects of fumed silica on the nonlinear tensile creep behavior of PP, (2) to construct the generalized creep curves by applying the time–strain and time–temperature superposition principles, (3) to substantiate the equivalence between the two approaches by comparing the correspondent creep master curves.

Experimental section

Materials and sample preparation

An isotactic polypropylene PPH-B-10-FB (MFI at 190 °C and 2.16 kg = 6.9 g/10 min, density = 0.904 g/cm^3) provided by Lati Industria Termoplastici S.p.A. (Varese, Italy) and produced by Polychim Industrie S.A.S. (Loon-Plage, France) was used in this work. Fusabond® P M-613-05 maleic anhydride-grafted polypropylene (PPgMA) (MFI at 190 °C and 2.16 kg = 106.8 g/10 min, density = 0.903 g/cm^3, maleic anhydride content = 0.35–0.70 wt%), was supplied by DuPont™ de Nemours (Geneva, Switzerland).

Both untreated and surface-treated fumed silica nanoparticles were supplied by Evonik Industries AG (Hanau, Germany). Untreated nanoparticles (Aerosil® A380) had an average primary particle size of 7 nm, a specific surface area of 321 ± 3 m^2/g. Dimethyldichlorosilane-functionalized silica nanoparticles (Aerosil® R974) were characterized by an average primary particle size of 12 nm, specific surface area of 124 ± 1 m^2/g.

Binary nanocomposites containing 5 wt % of both untreated and surface-treated silica nanoparticles were prepared by melt mixing in a Thermo Haake® internal mixer (T = 190 °C, n = 50 rpm, t = 10 min) followed by hot pressing using a Carver® hot press (T = 190 °C, p = 0.76 MPa, t = 10 min), to get plane sheets with thickness of around 0.7 mm. Ternary nanocomposites were prepared by adding 5 wt% of PPgMA as compatibilizer to the systems containing 5 wt% SiO_2. As a mean of comparison, binary composites containing 5 and 10 wt% of PPgMA were

also produced. Before melt processing, silica nanoparticles were dried for 24 h at 100 °C.

The unfilled matrix was denoted as PP, while nanocomposites were designated indicating the matrix, the compatibilizer (when present) with its content, the kind of filler and its amount. For instance, a sample filled with 5 wt% of silica Aerosil A380 is indicated as PP-A380-5.

Filler characterization

Density measurements were carried out by helium pycnometry (Micromeritics® Accupyc 1330 helium pycnometer, Norcross USA), at a temperature of 23 °C, using a testing chamber of 3.5 cm^3.

To evaluate the surface morphology of the fillers, BET (Brunauer, Emmett, Teller) surface area and porosity measurements were performed on silica nanoparticles Aerosil® R974, while these characterizations had been previously reported for Aerosil® A380 [43]. An ASAP® 2010 accelerated surface area and porosimetry machine (Norcross, USA) was utilized referring to the nitrogen gas physisorption process, setting a saturation pressure of 738.57 mmHg and a bath temperature of 77.35 K.

Composite characterization

Cryogenic fracture surfaces of PP nanocomposites were observed at various magnifications using a Zeiss Supra 40 (Berlin, Germany) field emission scanning electron microscope (FESEM), at an acceleration voltage between 2.5 and 4 kV. A thin silver coating was applied onto the surface by plasma sputtering to minimize the charging effects.

Transmission electron microscopy (TEM) was adopted to analyze cryocut thin sections of PP nanocomposites. A Philips® EM 400 T (Amsterdam, Netherlands) transmission electronic microscope was utilized at an acceleration voltage of 120 kV. Samples were prepared by cutting 70 nm-thin sections by a cryo-ultramicrotome UCT (Leica, Vienna, Austria) operating at −100 °C. Sections were collected on a 600-mesh copper grid.

Thermal analyses

Differential scanning calorimetry (DSC) tests were carried out by a Mettler® DSC30 differential scanning calorimeter under a constant nitrogen flow of 100 ml min^{-1}. The samples were first heated to 200 °C at a rate of 10 °C min^{-1} and held for 5 min to erase any previous thermal history. Crystallization tests at cooling rates of 10 °C min^{-1} down to 0 °C were also carried out. A subsequent (second) heating scan was performed at 10 °C min^{-1}. A melting enthalpy for 100 % crystalline isotactic PP of $\Delta H^0 = 209$ J g^{-1} was considered [44]. Moreover, the crystallinity χ_c of nanocomposite samples was calculated by taking the weight fraction of PP and PPgMA of the composites into account. The melting temperatures T_{m1} and T_{m2} were recorded during the first and second heating scan, respectively. The crystallization

enthalpy ΔH_c was measured by integrating the heat flow curve during the cooling scan.

Mechanical tests

Uniaxial tensile tests were performed with an Instron® 4502 (Norwood, USA) tensile testing machine on samples of at least five ISO 527 type 1BA specimens. Tests were carried out at a crosshead speed of 0.25 mm min^{-1} up to a maximum axial deformation of 1 %. The strain was recorded using a resistance extensometer Instron® model 2620-601 with a gage length of 12.5 mm. According to ISO 527 standard, the elastic modulus was measured as a secant value between deformation levels of 0.05 and 0.25 %.

Uniaxial tensile properties, such as stress at yield (σ_y), stress at break (σ_b) and strain at break (ε_b) were determined at a higher crosshead speed (5 mm min^{-1}) without extensometer.

Creep tests were performed utilizing a dynamic mechanical analyser DMA Q800 (TA Instruments®-Waters LLC, New Castle, USA) applying a constant stress (σ_0) of 3 MPa (i.e., 10 % of the stress at yield of unfilled PP) for 3,600 s at 30 °C. Rectangular samples 25 mm long, 5 mm wide and 0.20 mm thick were used, adopting a gage length of 11.5 mm. Noteworthy, specimens with lower thickness were chosen to perform creep tests at higher stress levels while maintaining the same instrument setup equipped with a 18 N load cell.

The creep compliance $D(t)$, computed as the ratio between the strain and the creep stress, was plotted against the time for the different samples. Since the samples PP-PPgMA-5-A380-5 and PP-PPgMA-5-R974-5 showed the best creep stability, creep tests were performed at 30 °C for 3,600 s under various applied stress levels σ_0 between 10 and 50 % of the stress at yield. Master curves were constructed by applying TSSP [24] ("Appendix").

Creep tests were also carried out imposing a constant stress of 3 MPa for 1,200 s and ranging the temperature between 30 and 70 °C, in 10 °C steps. The temperature range was properly chosen to remain within the linear viscoelastic region. Master creep curves were constructed by applying the TTSP according to the classical approach based on the Williams, Landel and Ferry (WLF) equation, setting a reference temperature T_0 of 30 °C.

Dynamic mechanical thermal analyses (DMTA) were carried out in tensile mode by the DMA Q800 testing machine on film specimens 25 mm long, 5 mm wide and 0.2 mm thick. First, some selected samples were analyzed over a temperature range between −20 and 160 °C, at a heating rate of 3 °C/min and a frequency of 1 Hz. A preload of 0.2 MPa and a maximum strain of 0.05 % were set for each test. The most important viscoelastic functions (E', E'', $\tan\delta$) were recorded at various temperatures. Multi-frequency DMA tests were carried out on PP, PP-PPgMA-5-A380-5 and PP-PPgMA-5-R974-5 samples, imposing a temperature step of 10 °C from −20 to 140 °C and setting the following test frequencies: 0.1, 0.32, 1, 3.2, 10, 31.6 and 100 Hz. Master curves were obtained according to a frequency–temperature superposition principle setting a reference temperature of 30 °C.

Results and discussion

Filler characterization

The density data obtained on fumed silica nanoparticles are reported in Table 1. For both samples, at least 300 measures were performed with the helium pycnometer to reach a constant density value. This behavior could probably be due to the open porosity present on the surface of fumed silica aggregates, among which helium molecules can penetrate and diffuse with difficulty. Surface-treated nanoparticles show a slightly lower density than untreated nanoparticles, probably because of the presence on the nanoparticles surface of hydrocarbon chains with a relatively low density.

The specific surface area was evaluated by the BET (Brunauer–Emmett–Teller) [45] method from the interpolation of the linear part of the adsorption curve in the plot reporting the adsorbed nitrogen volume versus the relative pressure (Table 1). Furthermore, following BJH (Barrett–Joiner–Holenda) [46] method, it was possible to determine the pore size distribution and the surface area contribution associated to pores of different dimensions. The data referring to Aerosil® A380 were reported from the literature [43]. The samples show significantly different BET surface area and BJH surface area of pores, while the average diameter of pores is similar.

Composites microstructure

The ESEM images of the fracture surface of PP-A380-5 and PP-R974-5 samples are represented in Fig. 1a, c, respectively. In the SEM micrographs of PP-silica samples, it can be seen that isodimensional aggregates appear distributed quite homogeneously within the matrix in both samples. The ESEM images of the fracture surfaces of PP-PPgMA-5-A380-5 and PP-PPgMA-5-R974-5 samples are shown in Fig. 1b, d, respectively. If compared with the corresponding nanocomposites prepared without the addition of PPgMA, the size of aggregates in ternary nanocomposites is markedly lower. The maleic anhydride group is supposed to act as a compatibilizing agent, breaking up the large filler aggregates and agglomerates into finer particles, resulting in a better dispersion within the polymer matrix,

Table 1 Density measurements and surface properties of silica nanoparticles

Sample	Density (g/cm^3)	BET surface area (m^2/g)[a]	BJH adsorption cumulative surface area of pores (1.7–300 nm) [m^2/g][b]	BJH adsorption average pore diameter (nm)[c]
Aerosil® A380	2.359 ± 0.017	320.8 ± 3.4	247.0	11.5
Aerosil® R974	2.298 ± 0.015	124.4 ± 0.6	129.0	12.9

[a] Surface area calculated according to Brunauer–Emmett–Teller method [1]

[b] Surface area associated to pores of different dimensions according to Barrett–Joiner–Holenda method [2]

[c] Average pore diameter computed according to Barrett–Joiner–Holenda method [2]

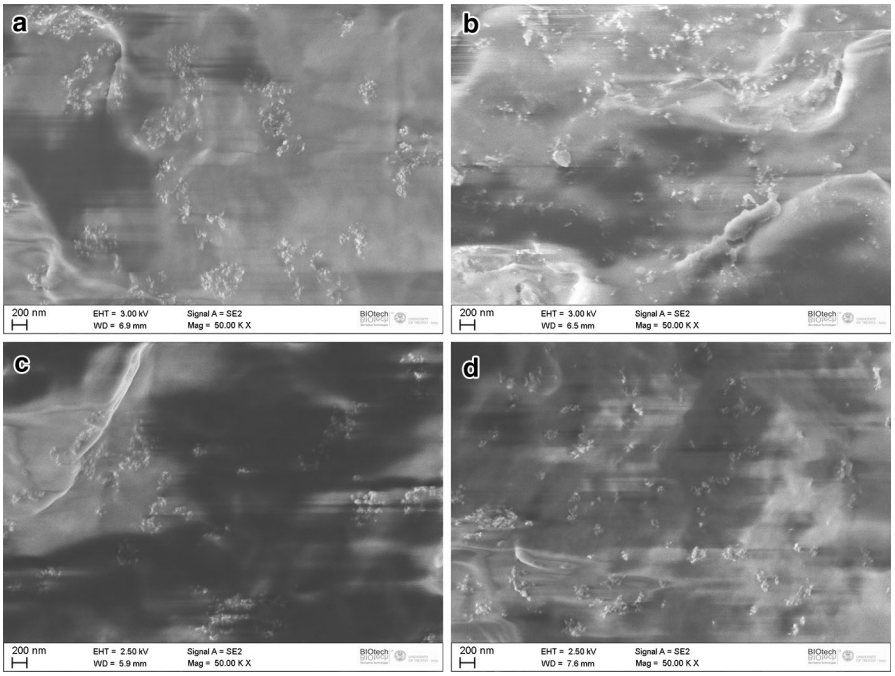

Fig. 1 ESEM images of the fracture surface of **a** PP-A380-5, **b** PP-PPgMA-5-A380-5, **c** PP-R974-5 and **d** PP-PPgMA-5-R974-5

accompanied with an increase in the interfacial adhesion [47]. Specifically, during the preparation of nanocomposites added with PPgMA, the hydroxyl groups present on the surface of silica nanoparticles may react as a nucleophile with the maleic anhydride groups of the compatibilizer [47], resulting in an increased compatibility of the filler with the macromolecular polymer chains and formation of smaller aggregates. Moreover, the reduction of aggregate dimensions can support the enhanced tensile and viscoelastic mechanical properties showed by nanocomposites containing PPgMA (Tables 4, 5).

TEM analyses corroborate the previous observations and allow an estimation of the aggregates dimension. In particular, from TEM micrographs, it is possible to clearly discern silica primary particles, spherical in shape and with a diameter between 10 and 20 nm, according to the produced datasheet (Fig. 2). As a comparison, the mean size of silica aggregates is summarized in Table 2.

Thermal analyses

The addition of silica produces a moderate increase of the crystallization temperature, which is further incremented by compatibilizer incorporation in the system containing silica A380. However, when the compatibilizer is added to the system containing silica R974, the crystallization temperature is slightly reduced.

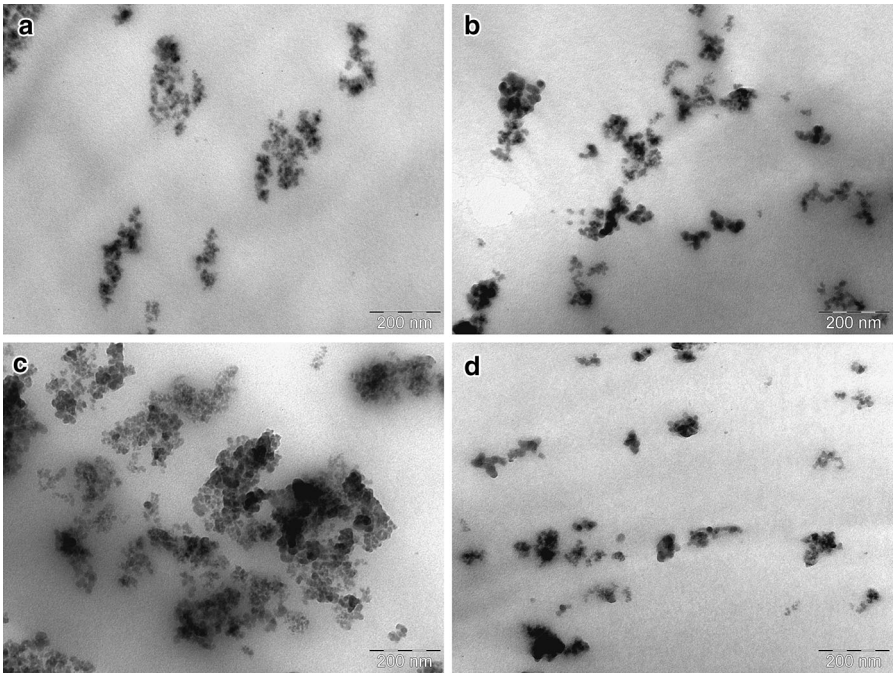

Fig. 2 TEM micrographs of cryocut surfaces of **a** PP-A380-5, **b** PP-PPgMA-5-A380-5, **c** PP-R974-5 and **d** PP-PPgMA-5-R974-5

Table 2 Mean aggregate size of PP-silica nanocomposites estimated from TEM analyses

Sample	Mean aggregate size (nm)
PP-A380-5	198 ± 15
PP-R974-5	171 ± 23
PP-PPgMA-5-A380-5	106 ± 9
PP-PPgMA-5-R974-5	91 ± 10

This decrease could be due to the increased interaction between the compatibilized PP and the silica nanoparticles, which may retard the migration of the PP chains onto the growing crystal nucleus. Concurrently, the melting temperature recorded during the second scan (T_{m2}) is slightly higher for PP nanocomposites, probably due to polymorphism (i.e., different crystalline forms with peculiar melting temperature are coexisting within the crystalline phase) induced by nanofiller incorporation [48]. Quite on the other hand, the crystallinity (χ_c) does not seem to have a direct correlation with the nanofiller addition (Table 3).

Mechanical response

As reported in Table 4, the addition of silica nanoparticles induces a remarkable increase of the elastic modulus of the PP matrix, which is further incremented by the

Table 3 DSC parameters on unfilled PP and relative nanocomposites

Sample	T_{m2} (°C)[a]	ΔH_c (J/g) [χ_c (%)][b]	Cryst. peak T (°C)[c]
PP	165.1	102.0 (48.8)	115.6
PP-PPgMA-5	163.1	100.7 (48.2)	117.0
PP-PPgMA-10	162.8	100.3 (48.0)	117.9
PP-A380-5	165.4	98.1 (49.4)	116.8
PP-R974-5	165.5	97.5 (49.1)	116.9
PP-PPgMA-5-A380-5	166.0	98.1 (48.4)	117.5
PP-PPgMA-5-R974-5	166.7	98.4 (49.6)	115.3

[a] Melting temperature recorded during the second scan

[b] Crystallization enthalpy (ΔH_c) and normalized crystallinity (χ_c)

[c] Crystallization peak temperature

Table 4 Elastic modulus and quasi-static tensile properties at yield and at break

Sample	Modulus (MPa)	Yield strength (MPa)	Stress at break (MPa)	Strain at break (%)
PP	1,546 ± 24	37.1 ± 0.1	35.0 ± 0.1	16.8 ± 0.3
PP-PPgMA-5	1,729 ± 31	36.7 ± 0.4	34.5 ± 0.6	13.3 ± 0.7
PP-PPgMA-10	1,648 ± 12	35.4 ± 0.4	33.6 ± 0.5	12.1 ± 0.6
PP-A380-5	1,698 ± 32	37.2 ± 0.5	35.5 ± 0.4	9.0 ± 0.4
PP-R974-5	1,865 ± 24	35.6 ± 0.5	33.6 ± 0.5	10.2 ± 0.7
PP-PPgMA-5-A380-5	2,015 ± 40	35.7 ± 0.4	34.2 ± 0.3	6.7 ± 0.2
PP-PPgMA-5-R974-5	2,281 ± 58	34.2 ± 0.4	31.3 ± 0.9	12.0 ± 1.1

incorporation of PPgMA, reaching an improvement of 47 % for ternary systems, compared to unfilled PP. Noteworthy, the systems produced with the addition of PPgMA showed an increase in elastic modulus comparable with that obtained with the introduction of nanoparticles, at the same weight content. In general, the yield strength and the stress at break decrease with the addition of the nanofiller for both kinds of silica nanocomposites, probably because of filler aggregation and stronger interaction [47]. For the same reason, the elongation at break exhibited by the nanocomposite is lower than that of unfilled PP.

In Fig. 3a, b, the isothermal creep compliance of unfilled PP and PP-silica nanocomposites, under a constant load of 3 MPa and at 30 °C, is reported, while in Table 5 the elastic (D_e) and total components of the creep compliance after 2,000 s ($D_{t2,000}$) are summarized. The introduction of silica nanoparticles leads to a significant improvement of the creep stability of the material. It is generally believed that nanoparticles can effectively restrict the motion of polymer chains, influencing the stress transfer at a nanoscale, with positive effects on the creep stability of the material [29]. Nevertheless, the creep compliances do not seem to significantly depend on the silica nanoparticle type.

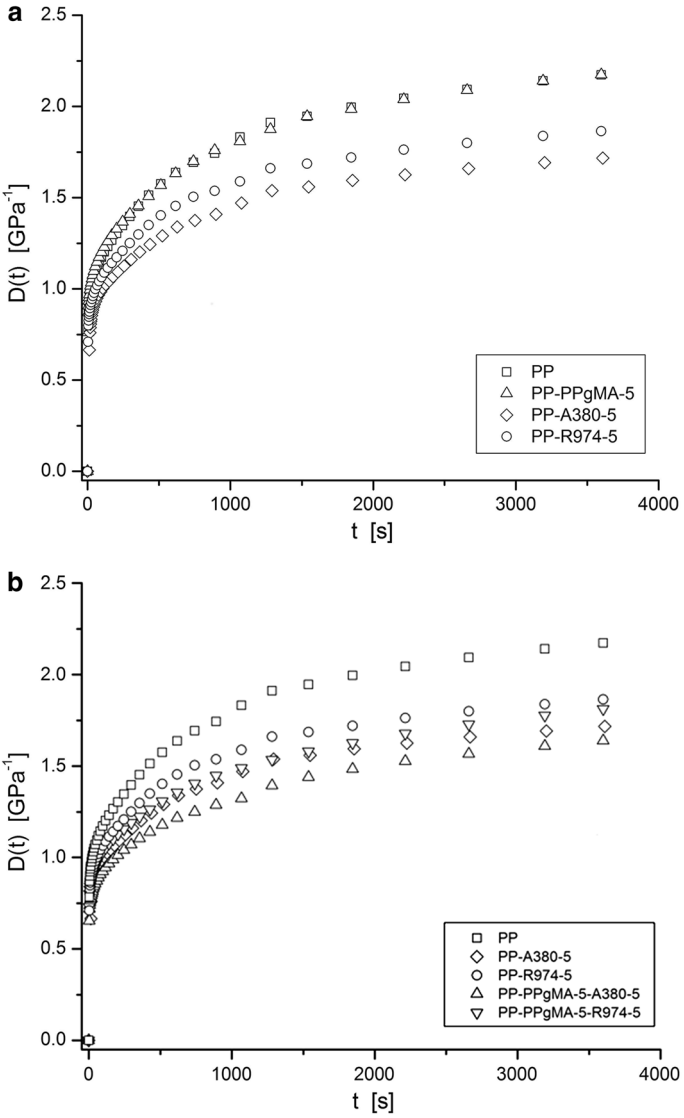

Fig. 3 Creep compliance $D(t)$ of **a** unfilled PP and PP-silica-5 nanocomposites, **b** PP-silica-5 and PP-PPgMA-5-silica-5 ($T = 30$ °C, $\sigma_0 = 3$ MPa)

Isothermal creep compliance master curves were constructed for the samples PP, PP-PPgMA-5-A380-5 and PP-PPgMA-5-R974-5 applying the TSSP at the reference stress. As proposed by Kolarik et al. [23, 28, 29], with a proper choice of the parameters (Table 6), it is possible to construct creep compliance master curves taking into account the nonlinear viscoelastic behavior of the material when relatively high stresses are applied.

Table 5 Elastic (D_e), viscoelastic ($D_{ve,2,000s}$) and total creep compliance at 2,000 s ($D_{t,2,000s}$) of PP nanocomposites

Sample	D_e (GPa^{-1})	$D_{ve,2,000s}$ (GPa^{-1})	$D_{tot,2,000s}$ (GPa^{-1})	$(D/D_0)_{tot,2,000s}$	$E_{a,creep}$ (KJ/mol)[a]
PP	0.85	1.24	2.09	–	209 ± 19
PP-PPgMA-5	0.82	1.22	2.04	0.98	–
PP-PPgMA-10	0.85	1.25	2.10	1.00	–
PP-A380-5	0.68	0.95	1.63	0.78	–
PP-R974-5	0.76	1.00	1.76	0.84	–
PP-PPgMA-5-A380-5	0.65	0.86	1.51	0.72	181 ± 17
PP-PPgMA-5-R974-5	0.72	0.91	1.63	0.78	182 ± 18

[a] Activation energy values obtained from the fitting of the shift factors used when applying the TTSP and according to the Arrhenius equation (Eq. 1)

Table 6 Parameter used for the evaluation of the nonlinear creep behavior of PP nanocomposites ("Appendix")

Parameter	Value
f_g	0.025
T_g (°C)	−16.40
T (°C)	30.00
α_{fv} (K^{-1})	0.000330
Δf_{Tc}	0.0153
x_c	0.488
v_2	0.488
v_{2cr}	0.156
q	1.800
M	1.589
ν	0.460
B	1.000

Representative creep compliance curves of unfilled PP at 30 °C are reported in Fig. 4a on double logarithmic scale for different applied stresses and they are compared with the theoretical ones, derived from the fitting according to the nonlinear tensile creep approach (solid lines). The fitting parameters, based on Eqs. 8 and 9, are summarized in Table 7 for PP and all PP nanocomposites. Since $\log(C^*)$ increases with the applied stress and the value of n^*, which should be independent on the applied stress (σ_0), shows very poor dependence on σ_0, the proposed approach appears to be quite suitable to study the dependence of the creep behavior on the applied stress for unfilled PP and relative silica nanocomposites. The master curve of PP, constructed according to strain-dependent shift factors $\log(a_\varepsilon)$, is depicted in Fig. 4b. Master curves of unfilled PP, PP-PPgMA-5-A380-5 and PP-PPgMA-5-R974-5 are shown in Fig. 5. The comparison highlights the better creep stability of PP nanocomposites with respect to neat PP, but not significative differences among PP nanocomposites.

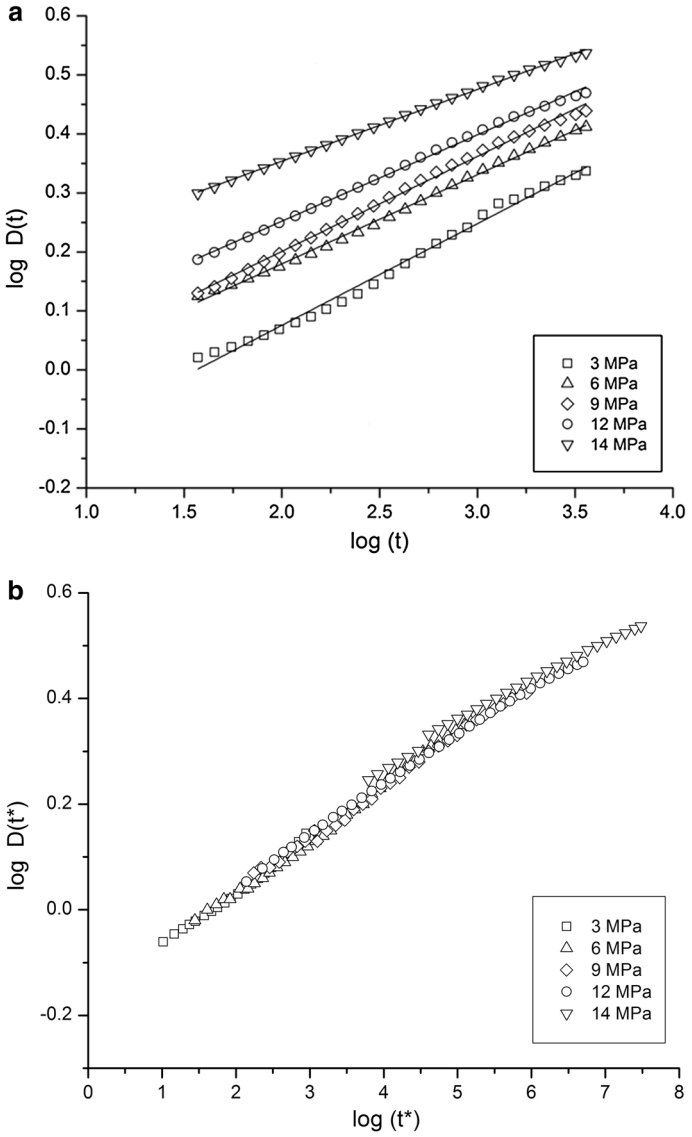

Fig. 4 **a** Representative creep compliance curves $D(t)$ at different creep stresses σ_0 and **b** superimposed creep curves according to the nonlinear tensile creep approach of unfilled PP ($T = 30$ °C)

Representative creep compliance curves of PP at temperatures ranging from 30 to 70 °C, under an applied stress of 3 MPa, are reported in Fig. 6a. Superimposed curves, constructed according to the TTSP and setting the reference temperature to 30 °C, are represented in Fig. 6b for PP and relative nanocomposites. The deformation behavior of the materials is strongly dependent on the temperature, while the introduction of silica nanoparticles leads to a significant decrease of the

Table 7 Fitting parameters of the creep data of PP nanocomposites according to the model presented in "Appendix"

σ_0 (MPa)	PP			PP-PPgMA-5-A380-5			PP-PPgMA-5-R974-5		
	log (C^*)	n^*	R^2	log (C^*)	n^*	R^2	log (C^*)	n^*	R^2
3	−0.269 ± 0.008	0.172 ± 0.003	0.990	−0.336 ± 0.008	0.153 ± 0.003	0.999	−0.284 ± 0.008	0.150 ± 0.003	0.999
6	−0.122 ± 0.004	0.151 ± 0.001	0.998	−0.268 ± 0.002	0.163 ± 0.002	0.999	−0.267 ± 0.006	0.152 ± 0.002	0.999
9	−0.121 ± 0.004	0.161 ± 0.002	0.997	−0.220 ± 0.004	0.179 ± 0.002	0.998	−0.264 ± 0.005	0.160 ± 0.002	0.996
12	−0.040 ± 0.004	0.146 ± 0.001	0.997	−0.218 ± 0.003	0.193 ± 0.001	0.997	−0.240 ± 0.003	0.168 ± 0.001	0.994
14	0.110 ± 0.002	0.122 ± 0.001	0.998	−0.098 ± 0.002	0.172 ± 0.001	0.990	−0.184 ± 0.003	0.179 ± 0.001	0.991

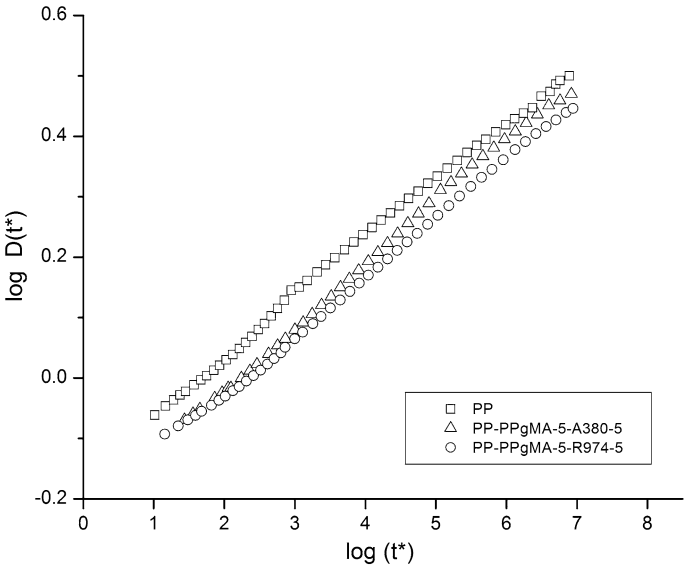

Fig. 5 Master curves of creep compliance $D(t)$, according to the nonlinear tensile creep superposition principle, of unfilled PP and PP-PPgMA-5-silica-5 nanocomposites ($T = 30$ °C)

creep compliance, which is more efficient when long creep times are considered and thus when high temperatures are taken into account.

To investigate the correlation between creep properties and polymeric chain dynamics, an analysis of the shift factors derived from the TTSP has been carried out.

Various polymeric materials are characterized by time–temperature shift factors following the Arrhenius relation (Eq. 1) for temperatures lower than the glass temperature and the Williams, Landel and Ferry equation (Eq. 2) for higher temperatures.

$$\ln a_{T_0}(T) = \frac{E_a}{R}\left(\frac{1}{T} - \frac{1}{T_0}\right) \tag{1}$$

$$\log a_{T_0}(T) = -\frac{C_1(T - T_0)}{C_2 + (T - T_0)} \tag{2}$$

Where E_a is an activation energy, R the ideal gas constant, and C_1 and C_2 are empirical constants depending on the material.

Activation energy values ($E_{a,creep}$) were obtained by applying the Arrhenius equation (Eq. 1) on a sufficiently linear trend of shift factors with respect to the reciprocal of the absolute temperature [49]. Due to the high uncertainty, activation energy values of the nanocomposites seem quite similar to that of unfilled PP (Table 5), indicating that the viscous flow of the polymer macromolecules does not significantly depend on the presence of the nanoparticles.

The equivalence between the time–strain and time–temperature superposition principle can be investigated by comparing the corresponding superimposed master curves (Fig. 7). Master curves obtained by the two different approaches appear quite

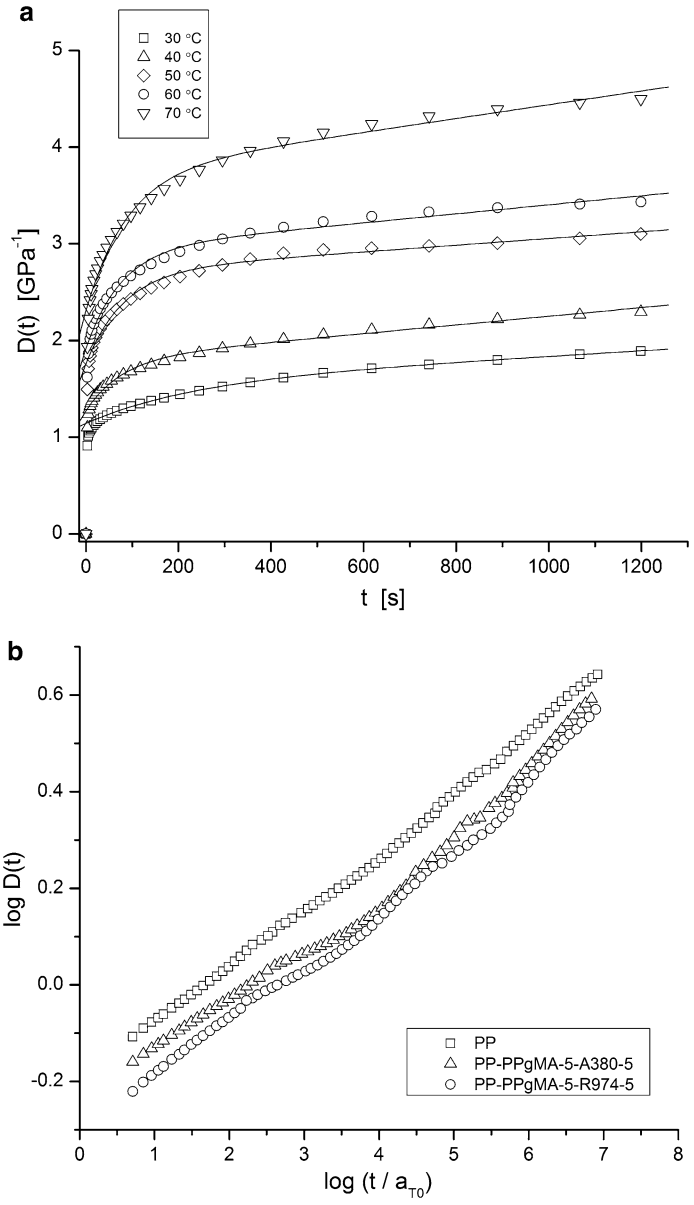

Fig. 6 **a** Representative creep compliance curves $D(t)$ at different temperatures of PP and **b** master curves of the creep compliance according to time–temperature superposition principle ($\sigma_0 = 3$ MPa, $T_0 = 30$ °C) of unfilled PP and PP-PPgMA-5-silica-5 nanocomposites

similar for both PP and relative nanocomposites over a wide range of reduced time. However, a slight divergence is manifested at very high reduced times (i.e., elevated temperature or high applied stresses), with the time–temperature data showing a significantly greater compliance compared to the time–strain data. The implication

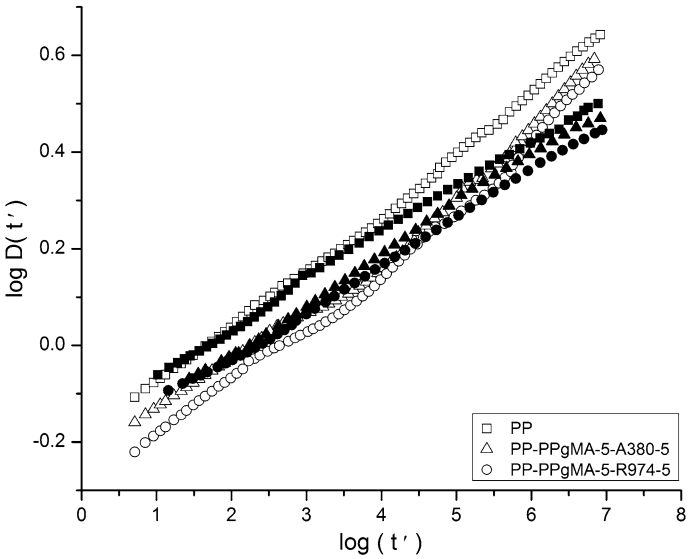

Fig. 7 Comparison of master curves according to the time–strain (*full point*) and time–temperature (*open point*) superposition principle of unfilled PP and PP-PPgMA-5-silica-5 nanocomposites

is that temperature and strain affect the creep response in different ways. Moreover, while the TSSP takes into account the underlying viscoelastic response function that is characteristic of the material, the TTSP does not contemplate a full description of the behavior of the material being tested. Further research needs to be done on the TTSP to take into account the characteristic parameters of the material and extend the applicability of the principle in the nonlinear viscoelastic region.

The introduction of the nanofiller produces an enhancement of E' both in the glassy and in the rubbery regions (Fig. 8a). During DMTA experiments, two peaks were observed on tanδ plot, identified as α and β relaxation, in order of decreasing temperature (Fig. 8b). The T_g of PP nanocomposites, usually referred to the β relaxation, is slightly higher than that of unfilled PP due to the presence of the nanofiller (Table 8), which decreases the mobility of the macromolecules. The sample PP-PPgMA-5-A380-5 shows a higher enhancement of the storage modulus than PP-PPgMA-5-R974-5, with respect to unfilled PP (Fig. 9a).

Superimposed curves of the storage modulus were constructed from the results of multi-frequency tests on the basis of a time–frequency superposition principle, considering as reference temperature T_0 of 30 °C.

The shift factors derived from the construction of the master curves are plotted in Fig. 9b. As already shown for the creep tests conducted at various temperatures, the Arrhenius equation (Eq. 1) was utilized to obtain activation energy (E_a) values (Table 8). However, since the shift factors for the construction of the E' master curves did not follow a good linearity over the whole range of the variable *1/T,* the points were properly divided into three regions and a stepwise linear fitting was carried out on each region. In this way, three activation energies were computed

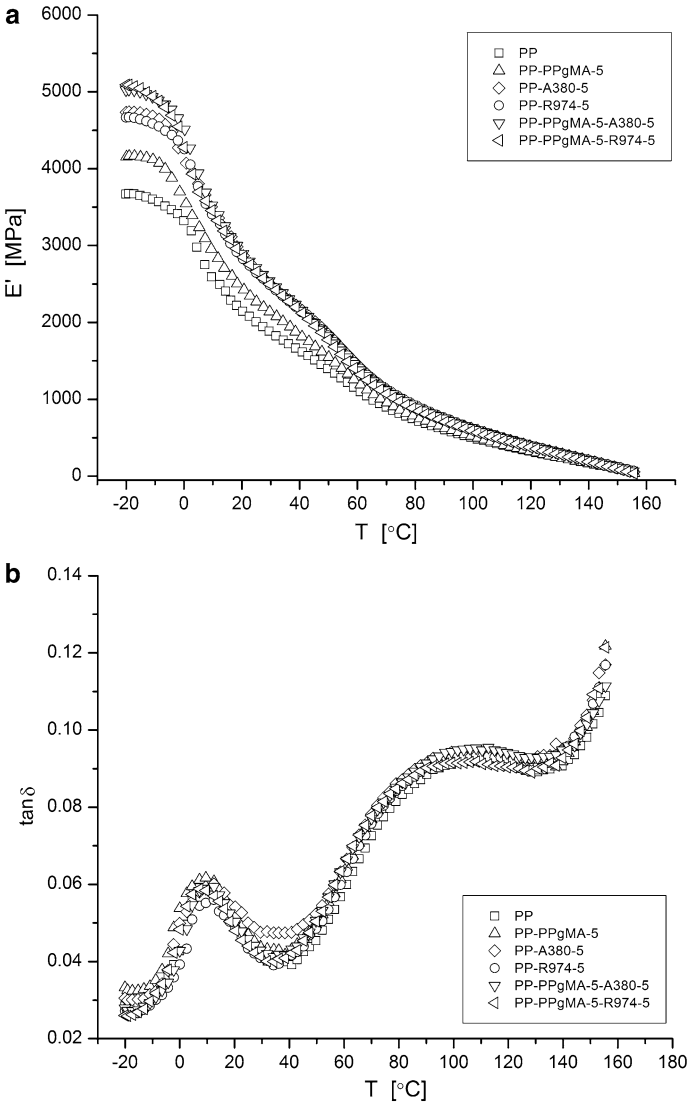

Fig. 8 Dynamic mechanical properties of unfilled PP and relative nanocomposites ($f = 1$ Hz): **a** storage modulus (E') and **b** loss tangent [tanδ]

($E_{a,1}$, $E_{a,2}$ and $E_{a,3}$), from the fitting of the regions of points going from higher to lower values of *1/T*.

E_a values of PP nanocomposites seem quite similar to those of unfilled PP because of being affected by high uncertainty, confirming that the viscous flow of PP macromolecules is not significantly affected by the presence of the nanoparticles. The activation energy values computed from multi-frequency DMTA tests are quite similar to those found for the creep tests ($E_{a,creep}$) especially when considering $E_{a,1}$ and $E_{a,2}$. Interestingly, activation energy values related to the

Table 8 Dynamic mechanical properties ($f = 1$ Hz) and activation energy values of unfilled PP and relative nanocomposites

Sample	E' (−20 °C) [MPa]	E' (23 °C) [MPa]	E'' (23 °C) [MPa]	$T_{\beta peak}$ (°C)[a]	E_a (kJ/mol)[b]
PP	3,674.4	2,063.1	90.3	9.9	231 ± 8
					183 ± 4
					295 ± 21
PP-PPgMA-5	4,155.1	2,340.0	115.3	9.1	–
PP-PPgMA-10	3,925.2	2,268.3	108.7	9.1	–
PP-A380-5	4,733.7	2,756.1	141.7	11.8	–
PP-R974-5	4,668.1	2,727.5	125.3	11.4	–
PP-PPgMA-5-A380-5	5,025.8	2,777.1	131.6	11.3	210 ± 9
					171 ± 2
					286 ± 22
PP-PPgMA-5 R974-5	5,092.2	2,749.9	123.5	11.2	220 ± 4
					167 ± 4
					287 ± 22

[a] Temperature correspondent to the β peak recorded in tanδ plot

[b] Activation energy values E_{a1}, E_{a2} and E_{a3} listed from top to bottom

viscous flow of macromolecules show good concordance when derived from creep and dynamic regime tests.

Conclusions

The addition of PPgMA resulted in a better dispersion of silica nanoparticles (both untreated and surface treated) within the PP matrix, as confirmed by ESEM and TEM observations, inducing a remarkable improvement of the tensile mechanical properties, as measured through quasi-static tensile tests. Untreated nanoparticles at elevated surface area resulted to be effective in increasing elastic modulus, because of the extended filler–matrix interaction, while the finer dispersion of silica aggregates at the nanoscale level obtained using surface-treated nanoparticles produces even greater improvements of the elastic modulus.

The nonlinear viscoelastic creep of the composites, successfully studied by the application of the time–strain superposition principle, showed a considerable enhancement of the creep stability in nanocomposites with respect to unfilled PP, especially for higher creep stresses, but no significative differences between nanocomposites filled with different nanosilicas.

The study of creep dependence on the temperature showed that the stabilizing effect provided by the nanoparticles was more effective at high temperatures and, considering the time–temperature superposition principle, at long loading times.

The equivalence between the time–strain and time–temperature superposition principle was substantiated by comparing the correspondent superimposed master

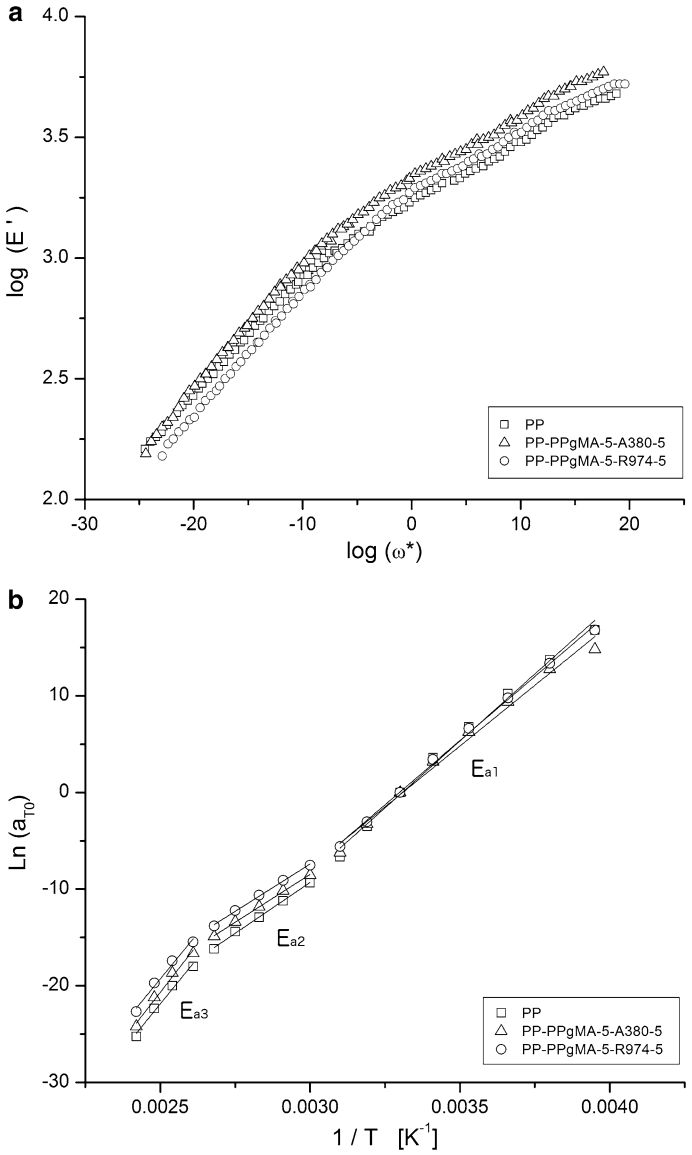

Fig. 9 **a** Comparison between master curves of E' obtained by multi-frequency tests on PP-silica nanocomposites ($T_0 = 30$ °C) and **b** shift factors for the construction of the E' master curves with stepwise linear fitting according to Arrhenius equation (Eq. 1)

curves. To gain some insight on the correlation between creep properties and polymeric chain dynamics, activation energy values were obtained by the analysis of the shift factors derived from the TTSP. Both storage and loss modulus, measured through DMA tests, were enhanced in all nanocomposites, observing a maximum storage modulus for samples with 5 wt% PPgMA and 5 wt% surface-treated silica.

Activation energy values obtained from the elaboration of multi-frequency tests were in good agreement with those referred to creep tests.

Appendix

The strain in tensile creep, $\varepsilon(t,\ \sigma,\ T)$, generally depends on time t, stress σ, and temperature T, and can be expressed as the sum of the elastic (reversible, instantaneous) $\varepsilon_e(\sigma,\ T)$, viscoelastic (reversible, time-dependent) $\varepsilon_v(t,\ \sigma,\ T)$ and plastic $\varepsilon_p(t,\ \sigma,\ T)$ parts:

$$\varepsilon(t,\sigma,T) = \varepsilon_{\mathrm{e}}(\sigma,T) + \varepsilon_{\mathrm{v}}(t,\sigma,T) + \varepsilon_{\mathrm{p}}(t,\sigma,T) \tag{3}$$

The tensile compliance $D(t,\sigma) = \varepsilon(t,\ \sigma)/\sigma$ considered during isothermal nonlinear creep with no plastic deformation, can be written as follows:

$$D(t,\sigma) = D_{\mathrm{e}}(\sigma) + D_{\mathrm{V}}(t,\sigma) \tag{4}$$

A simple equation based on the retardation time approach was found suitable for describing isothermal creep of polypropylene and of its blends [23, 24, 27–29]:

$$\log D(t,\sigma) = \log W(\sigma) + n\log\left(\frac{t}{\tau_{\mathrm{rm}}}\right) \tag{5}$$

where $W(\sigma)$ is a function of stress, τ_{rm} is the mean retardation time and $0 \le n \le 1$ is the shape parameter indicating the distribution of retardation times.

The time–strain shift factor, $\log a_\varepsilon(t)$, defined as the ratio of the mean retardation time τ_{rm} $[\varepsilon(t),\ T_c]$ at a strain $\varepsilon(t)$ and τ_{rmi} $[\varepsilon_{\mathrm{i}} = 0,\ T_{\mathrm{c}}]$ for initial time $t_{\mathrm{i}} = 0$ (at a constant temperature T_{c}) can be obtained as [10]:

$$\log a_\varepsilon(t) = -\left(\frac{B}{2.303}\right)\frac{\left[(1-2v)M\varepsilon(t)/(f_{\mathrm{g}} + \Delta f_{T_{\mathrm{c}}})\right]}{\left[(1-2v)M\varepsilon(t) + (f_{\mathrm{g}} + \Delta f_{T_{\mathrm{c}}})\right]} \tag{6}$$

Where B is a numerical factor related to the ratio of the volume of a jumping segment to the volume of the critical vacancy necessary for the implementation of a segment jump, v is the Poisson's ratio, M is the ratio of the average strain of the creeping phase in the multiphase test specimen and the measured strain. The fractional free volume of the glassy state is defined as f_{g} and for most polymers the glassy state is considered as iso-free-volume state with $f_{\mathrm{g}} = 0.025$. If only the effects of temperature T and of strain $\varepsilon(t)$ are considered, the fractional free volume can be expressed as:

$$f(t,\varepsilon(t)) = f_{\mathrm{g}} + \alpha_{fv}\left(T - T_{\mathrm{g}}\right) + (1-2v)\varepsilon(t) = f_{\mathrm{g}} + \Delta f_{\mathrm{T}} + \Delta f_{\varepsilon} \tag{7}$$

Where α_{fv} is the expansion coefficient of the free volume at $T > T_{\mathrm{g}}$, ν is Poisson's ratio and $[(1-2v)\ \varepsilon(t)]$ is the strain-induced dilatation for an isotropic material. The compliance can be expressed in logarithmic form as:

$$\log D(t,\sigma) = [\log W(\sigma) - n\log\tau_{\mathrm{rmi}}] + n[\log(t) - \log a_\varepsilon(t)] = \log C^* + n^*\log(t^*) \tag{8}$$

Where the parameters C^* and n^* refer to the internal time t^*, defined as:

$$\log(t^*) = \log(t) + \log a_\varepsilon(t) = \log(t) + \left(\frac{B}{2.303}\right)\frac{\left[(1-2\nu)M\varepsilon(t)/(f_g + \Delta f_{T_c})\right]}{\left[(1-2\nu)M\varepsilon(t) + (f_g + \Delta f_{T_c})\right]} \tag{9}$$

References

1. Streller RC, Thomann R, Torno O, Mülhaupt R (2008) Isotactic poly(propylene) nanocomposites based upon boehmite nanofillers. Macromol Mater Eng 293(3):218–227. doi:10.1002/mame.200700354
2. Mittal V (2007) Polypropylene-layered silicate nanocomposites: filler matrix interactions and mechanical properties. J Thermoplast Compos Mater 20(6):575–599. doi:10.1177/0892705707083636
3. Xanthos M (2010) Functional fillers for plastics. Wiley VCH, Weinheim
4. Dorigato A, Pegoretti A (2012) Fracture behaviour of linear low density polyethylene—fumed silica composites. Eng Fract Mech 79(1):213–224. doi:10.1016/j.engfracmech.2011.10.014
5. Pustak A, Smit I, Svab I (2008) V M Silica-reinforced polypropylene composites. Microscopy-advanced tools for tomorrow's materials. Springer, Berlin
6. Móczó J, Pukánszky B (2008) Polymer micro and nanocomposites: structure, interactions, properties. J Ind Eng Chem 14(5):535–563. doi:10.1016/j.jiec.2008.06.011
7. Bondioli F, Dorigato A, Fabbri P, Messori M, Pegoretti A (2009) Improving the creep stability of high density polyethylene by acicular titania nanoparticles. J Appl Polym Sci 112(2):1045–1055. doi:10.1002/app.29472
8. Pedrazzoli D, Pegoretti A (2013) Silica nanoparticles as coupling agents for polypropylene/glass composites. Compos Sci Technol 76(4):77–83. doi:10.1016/j.compscitech.2012.12.016
9. Pedrazzoli D, Dorigato A, Pegoretti A (2010) Monitoring the mechanical behaviour of electrically conductive polymer nanocomposites under ramp and creep conditions. J Nanosci Nanotechnol 12(5):4093–4102
10. Dorigato A, Pegoretti A, Kolařík J (2010) Nonlinear tensile creep of linear low density polyethylene/fumed silica nanocomposites: time–strain superposition and creep prediction. Polym Compos 31(11):1947–1955. doi:10.1002/pc.20993
11. Starkova O, Yang J, Zhang Z (2007) Application of time–stress superposition to nonlinear creep of polyamide 66 filled with nanoparticles of various sizes. Compos Sci Technol 67(13):2691–2698. doi:10.1016/j.compscitech.2007.02.014
12. Yang J-L, Zhang Z, Schlarb AK, Friedrich K (2006) On the characterization of tensile creep resistance of polyamide 66 nanocomposites. part II. modeling and prediction of long-term performance. Polymer 47(19):6745–6758. doi:10.1016/j.polymer.2006.07.060
13. Zhang Z, Yang J-L, Friedrich K (2004) Creep resistant polymeric nanocomposites. Polymer 45(10):3481–3485. doi:10.1016/j.polymer.2004.03.004
14. Siengchin S, Karger-Kocsis J, Thomann R (2007) Alumina-filled polystyrene micro- and nanocomposites prepared by melt mixing with and without latex precompounding: structure and properties. J Appl Polym Sci 105(5):2963–2972. doi:10.1002/app.26505
15. Siengchin S (2009) Long- and short-term creep of polyoxymethylene/polyurethane/alumina ternary composites by comparison. Mech Compos Mater 45(4):415–422. doi:10.1007/s11029-009-9091-8
16. Wang ZD, Zhao XX (2008) Modeling and characterization of viscoelasticity of PI/SiO2 nanocomposite films under constant and fatigue loading. Mater Sci Eng A 486(1–2):517–527. doi:10.1016/j.msea.2007.09.041
17. Dorigato A (2009) Viscoelastic and fracture behaviour of polyolefin based nanocomposites. Ph.D. thesis, University of Trento, Italy
18. Siengchin S, Haag R, Sinpayakun P (2009) A review of creep resistance of nano-scale reinforcing thermoplastics. Asian Int J Sci Technol 2:15–20
19. Pegoretti A (2009) Creep and fatigue behaviour of polymer nanocomposites. In: Karger-Kocsis J, Fakirov S (eds) Nano- and Micromechanics of Polymer Blends and Composites. Carl Hanser Verlag GmbH & Co. KG, Munich, pp 301–339

20. Karian H (2003) Handbook of polypropylene and polypropylene composites. Marcel Dekker, New York
21. Banik K, Karger-Kocsis J, Abraham T (2008) Flexural creep of all-polypropylene composites: model analysis. Polym Eng Sci 48(5):941–948. doi:10.1002/pen.21041
22. Andrew W (1991) The effect of creep and other time related factors on plastics and elastomers. Plastics Design Library, New York
23. Kolarik J, Pegoretti A, Fambri L, Penati A (2003) Prediction of non-linear long-term tensile creep of heterogeneous blends: rubber-toughened polypropylene-poly(styrene-co-acrylonitrile). J Appl Polym Sci 88(3):641–651. doi:10.1002/app.11586
24. Kolarik J, Fambri L, Pegoretti A, Penati A, Goberti P (2002) Prediction of the creep of heterogeneous polymer blends: rubber-toughened polypropylene/poly(styrene-co-acrylonitrile). Polym Eng Sci 42(1):161–169
25. Read BE, Dean GD, Tomlins PE (1988) Effects of physical ageing on creep in polypropylene. Polymer 29(12):2159–2169
26. Tomlins PE, Read BE (1997) Creep and physical ageing of polypropylene: a comparison of models. Polymer 39(2):355–367
27. Kolarik J (2003) Tensile creep of thermoplastics: time–strain superposition of non-iso free-volume data. J Polym Sci B Polym Phys 41:736–748
28. Kolařík J, Pegoretti A, Fambri L, Penati A (2003) Non-linear long-term tensile creep of poly(propylene)/cycloolefin copolymer blends with fibrous structure. Macromol Mater Eng 288(8):629–641. doi:10.1002/mame.200300005
29. Kolarik J, Pegoretti A (2006) Non-linear tensile creep of polypropylene: time–strain superposition and creep prediction. Polymer 47(1):346–356. doi:10.1016/j.polymer.2005.11.013
30. Ferry JD (1980) Viscoelastic properties of polymers. Wiley, New York
31. Lakes RS (1999) Viscoelastic solids. CRC Press, London
32. Moore DR, Turner S (2001) Mechanical evaluation strategies for plastics. Cambridge
33. Nielsen LE, Landel RF (1994) Mechanical properties of polymers and composites. New York
34. Rodriguez F (1996) Principles of polymer systems. Taylor and Francis, Washington DC
35. Ward IM, Hadley DW (1993) An Introduction to the mechanical properties of solid polymers. John Wiley & Sons, Chichester
36. McKeen LW (2009) The effect of creep and other related factors on plastics and elastomers. PDS handbook series, Oxford
37. Betten J (2005) Creep mechanics. Springer, Berlin
38. Matsumoto DS (2004) Time–temperature superposition and physical aging in amorphous polymers. Polym Eng Sci 28(20):1313–1317
39. Tajvidi M, Falk RH, Hermanson JC (2005) Time–temperature superposition principle applied to a kenaf-fiber/high-density polyethylene composite. J Appl Polym Sci 97(5):1995–2004. doi:10.1002/app.21648
40. Yeow YT (1978) The time–temperature behavior of graphite epoxy laminates. Virginia Polytechnic institute and state university, Blacksburg
41. Struik LCE (1989) Mechanical behaviour and physical ageing of semi-crystalline polymers: 3. prediction of long term creep from short time tests. Polymer 30(5):799–814
42. O'Connell PA, McKenna GB (1997) Large deformation response of polycarbonate: time–temperature time–aging time and time–strain superposition. Polym Eng Sci 37(9):1485–1495
43. Dorigato A, Dzenis Y, Pegoretti A (2011) Nanofiller aggregation as reinforcing mechanism in nanocomposites. Proc Eng 10:894–899. doi:10.1016/j.proeng.2011.04.147
44. James E (1999) Polymer data handbook. Oxford University Press, New York
45. Brunauer S, Emmett PH, Edward T (1938) Adsorption of gases in multimolecular layers. J Am Chem Soc 60:309–319
46. Barrett E, Leslie G, Halenda P (1951) The determination of pore volume and area distributions in porous substances. I. computations from nitrogen isotherms. J Am Chem Soc 73:373–380
47. Bikiaris DN, Vassiliou A, Pavlidou E, Karayannidis GP (2005) Compatibilisation effect of PP-g-MA copolymer on iPP/SiO2 nanocomposites prepared by melt mixing. Eur Polymer J 41(9):1965–1978. doi:10.1016/j.eurpolymj.2005.03.008
48. Karger-Kocsis J, Siengchin S (2014) Single-polymer composites: concepts, realization and outlook: review KMUTNB. Int J Appl Sci Technol 7(1):1–9. doi:10.14416/j.ijast.2014.01.002
49. Turi A (1997) Thermal characterization of polymeric materials, vol 1 and 2, 2nd edn. Academic Press, New York